Journal of Environmental Chemical Engineering 9 (2021) 106604

Contents lists available at ScienceDirect

Journal of Environmental Chemical Engineering

journal homepage: www.elsevier.com/locate/jece

River driftwood pretreated via hydrothermal carbonization as a sustainable source of hard carbon for Na-ion battery anodes

Abdullah F. Qatarneh [a,*], Capucine Dupont [a], Julie Michel [a,b], Loïc Simonin [b], Adrian Beda [c,d,e], Camelia Matei Ghimbeu [c,d,e], Virginia Ruiz-Villanueva [f], Denilson da Silva [g], Hervé Piégay [h], Mário J. Franca [a,i]

[a] IHE Delft Institute for Water Education, Westvest 7, 2611AX Delft, The Netherlands
[b] CEA, LITEN, DEHT, Université Grenoble Alpes, 17 rue des Martyrs, 38054 Grenoble CEDEX 9, France
[c] Université de Haute-Alsace, Institut de Science des Matériaux de Mulhouse, CNRS UMR 7361, F-68100 Mulhouse, France
[d] Université de Strasbourg, F-67081 Strasbourg, France
[e] Réseau sur le Stockage Electrochimique de l'Energie (RS2E), CNRS FR3459, 33 Rue Saint Leu, 80039 Amiens Cedex, France
[f] University of Lausanne, Lausanne, Switzerland
[g] FCBA, InTechFibres/BIOSENSE Division, Domaine Universitaire, CS 90251, 38044 Grenoble, France
[h] University of Lyon, CNRS UMR 5600, EVS - ENS Lyon, Lyon F-69363, France
[i] Delft University of Technology, Delft, Netherlands

ARTICLE INFO

Keywords:
Driftwood
Hydrothermal carbonization
Hydrochar
Hard carbon
Na-ion batteries

ABSTRACT

Producing hard carbon from lignocellulosic biomass has been the focus of recent studies as a promising source of anode material for Na-ion batteries. Woody biomass is a potential source, but it is already well valorized. Consequently, river driftwood can be an excellent alternative, especially since it is a disturbing waste for dam regulators. It can jeopardize dam safety, damage intake works, and sink in reservoirs, lowering water quality and decreasing reservoir volume. We examine the potential of river driftwood as a source of hard carbon for Na-ion batteries. Hydrothermal carbonization (HTC) was carried out at temperatures between 180 and 220 °C as the first step to produce hydrochar followed by an upgrading pyrolysis step at 1400 °C under an inert atmosphere to obtain hard carbon. We investigated the effect of HTC operational conditions and driftwood biomass (genera) on hydrochar and hard carbon properties, as well as the latter's impact on Na-ion batteries. The produced carbon electrodes delivered a reversible capacity of 270–300 mAh·g^{-1} for the first cycle and showed high coulombic efficiencies of 77–83%. We also observed promising cyclability of a maximum 2% loss after 100 cycles. Moreover, results suggest that obtained hard carbon can compete with commercial materials and is capable to supply large battery factories with anode material.

1. Introduction

The energy demand continues to rise steadily and globally, with a consequent rise in energy-related carbon emissions. The energy industry faces hence the challenge to cope with the increasing demand for energy and at the same time to reduce the energy-related greenhouse emissions. This development validates the current shift toward renewable energy sources, such as wind, solar and hydropower. The variability and unpredictability of these sources impose a need for energy buffers that can guarantee electrical grid stability for consumers. Chemical storage in the form of batteries provides one of these possibilities. Nowadays, an increasing number of consumer products, such as electric vehicles, mobile phones and laptops, are powered by electricity, with increasing demand for storage in the form of batteries, most notably Li-ion batteries [27].

The increase in demand is principally due to the rapid growth of electric vehicles sales, which currently account for 64% of the total Li-ion battery market and will grow to 90% in 2030 [31]. This growth resulted in a significant increase in the cost of raw materials for Li-ion batteries, sparking interest in Na-ion batteries because of their widely available and cheaper resources [56]. As graphite poorly reacts with Na ions, the most commonly used negative electrode material (anode) is

* Corresponding author.
E-mail address: abdullah.qatarneh@gmail.com (A.F. Qatarneh).

https://doi.org/10.1016/j.jece.2021.106604
Received 21 June 2021; Received in revised form 7 October 2021; Accepted 14 October 2021
Available online 19 October 2021

hard carbon. Hard carbon provides high storage capacity and cycling stability [11]. However, it is generally produced from fossil and expensive polymer precursors with a price per kg two to three times higher than graphite [37]. The high price is one of the most significant barriers to the widespread commercialization of this battery technology. In this regard, bio-based precursors appear to be of great interest for the production of these types of materials, especially if these precursors are underutilized.

Hard carbon can be produced from different types of materials including waste material, as different as Old-loofah [55], cigarette butts [16], and lignocellulosic biomass. Hard carbon material is derived through thermochemical processing, commonly by two steps [34]. The first step leads to the production of char material using either pyrolysis (typically around 500 °C) or Hydrothermal Carbonization (HTC) followed by a second upgrading pyrolysis step at high temperature (typically 900–1500 °C) [27].

Most studies on lignocellulosic biomass have adopted the more mature technology of one pyrolysis step, such as date palm [18] and pinecone [57]. On the other hand, an increasing number of studies is investigating the use of HTC as a first step, followed by pyrolysis such as, holly leaves [59] and peanut skin [47].

Recent studies have demonstrated that hard carbon obtained using HTC as a first step has a significantly better anode performance in Na-ion batteries when compared to pyrolysis. However, there is no agreement in the literature in the explanation behind it [27]. Wang et al. [47] attributed the enhanced initial capacity when HTC is used in hard carbon derived from peanut skin to the presence of significant micropores and mesopores. Zheng et al. [59] found that the higher microporosity introduced by HTC played an important role in enhancing its electrochemical performance of hard carbon derived from holly leaves. In addition, HTC is known to partially remove inorganic elements contained initially in the feedstock [19], which could explain the enhanced performances in Na-ion batteries. Indeed, a study by Saavedra Rios [35] found that high ash content, and especially the content of some specific inorganic elements, such as Si, and Ca, seem to impact battery performances. Similarly, a study by Susanti et al., [46] showed the positive effect of ash removal by acid pretreatment in the resulting hard carbon performances in Na-ion batteries.

This background shows the importance of finding low cost, highly available and low-ash-content biomass precursors to obtain affordable, efficient and sustainable hard carbon anodes.

The construction of an impounding structure across a valley interrupts the natural catchment fluxes that include the transport of wood recruited in the river slopes and conveyed by the river channel network. Driftwood hinders water abstraction from dams for human consumption, irrigation, and hydro-power generation. The driftwood accumulates upstream of these structures, with consequences to the safety and operation of their ancillary works. Furthermore, driftwood can sink to the reservoir's bottom, affecting water quality and reducing available volume for water storage. The extracted driftwood is a burden for dam regulators and is underused, often processed by combustion or dumped in landfills [1]. The accumulation of river driftwood upstream of dams is reported in many parts of the world with volumes up to millions of cubic meters, as the 2.2 million m^3 reported in Bratsk, Russia [21].

River driftwood has similar properties to classical wood but with the advantage of naturally gathering in a few collection points (dams and river singularities), facilitating its extraction. As shown above, river driftwood is currently often extracted upstream of dams and underused as a resource. However, driftwood is immersed in water and therefore is collected with a moisture content of around 60%, complicating its processing via thermochemical processes given the drying energy and cost needed [1]. For such wet biomass, HTC is a favorable option for char production since the process takes place in water and therefore benefits from the water content of the material.

To our knowledge, neither the behavior of river driftwood during HTC nor its conversion to hard carbon and use in Na-ion batteries have been studied before. Moreover, the impact of HTC operational conditions on hard carbon has never been extensively studied. Here, we intend to fill in this gap via an interdisciplinary study covering the whole value chain from hydrochar production from river driftwood to conversion in hard carbon and use in Na-ion battery. The river driftwood is collected upstream of the Génissiat dam, located on the Rhône River in France, where every year 2234 m^3 is extracted. We discuss the potential of this value chain in terms of Na-ion battery factory supply by river driftwood.

The paper is hence three folded. At first, we examine hydrochar production and properties related under different HTC operational conditions (temperature, residence time) and for various river driftwood biomass genera (*Conifer, Salix, Fraxinus, Populus* and *Alnus)*. Secondly, we provide an extensive physico-chemical characterization of the produced hard carbon. Lastly, we investigate the electrochemical performance of obtained hard carbon in Na-ion batteries, and we discuss the possible supply of battery factories by river driftwood.

2. Materials and methods

2.1. Case study

The Génissiat dam is located on the Rhône River in France, 50 km downstream from Geneva (Switzerland) and 160 km upstream from Lyon presents a case study where annually approximately 1300 tons of driftwood is extracted. The dam forms a reservoir stretching 23 km to the Swiss border. Lake Geneva (Lac Léman) impedes the transfer of wood and sediments from the upper Rhone to the dam. Yet, driftwood at Génissiat is supplied mainly during floods along the Rhône River and its two main tributaries downstream of Lake Geneva: The Arve and Valserine Rivers.

Floating wood blocked upstream of Génissiat dam usually has been in the water for a few weeks. Floating driftwood must be extracted mechanically to prevent sinking into the bottom of the reservoir. The sinking of wood can lead to significant accumulation posing safety and ecological risks. At Génissiat dam, the extracted driftwood is stored in a facility nearby the dam and later is used for energy production.

The average driftwood volume extracted annually over nine years from the dam based on Gouton [15] in the period between 2011 and July 2019 is an annual average of 2234 m^3 (maximum of 5234 m^3; minimum 700 m^3) of driftwood. For further details on the case study see Qatarneh et al. [32].

2.2. Feedstock

The sampling was conducted at the storage facility near to Génissiat dam. Briefly, five genera of driftwood were identified based on wood anatomical characteristics, i.e., cell patterns and wood features of polished samples using a microscope [39]. Identified genera were *Conifer, Salix, Fraxinus*, *Populus* and *Alnus*. *Alnus* driftwood samples were used to investigate the impact of operational conditions (residence time and temperature). The selection of *Alnus* is due to their high frequency in the Génissiat dam [15]. *Conifer, Fraxinus, Populus*, *Salix*, *Alnus* and *Alnus* bark were used to investigate the impact of driftwood composition on HTC. All driftwood samples were milled below 1 mm and dried at 105 °C for at least 24 h. As mentioned above, in an HTC process, such drying is not required and was carried out here to make the comparison easier between samples when keeping a constant feedstock/water ratio. The macromolecular composition of driftwood biomass is shown in Table 1 derived from Qatarneh et al. [32]. The comprehensive physicochemical properties of the feedstock have been measured in a previous study by Qatarneh et al. [32].

Table 1
Macromolecular composition (%) of driftwood biomass collected from Génissiat dam based on dry basis.

Genus	Cellulose	Hemicelluloses	Lignin (%)			Extractives (%)
			Klason	Soluble	Total	Total
Conifer	40.4 ± 0.2	29.3 ± 0.1	27.4 ± 0.2	0.2 ± 0.0	27.7 ± 0.2	2.9 ± 0.0
Fraxinus	41.0 ± 0.3	26.5 ± 0.5	23.8 ± 0.3	2.9 ± 0.0	26.8 ± 0.3	3.3 ± 0.0
Populus	43.9 ± 0.2	22.5 ± 0.2	23.1 ± 0.1	2.0 ± 0.0	25.1 ± 0.1	4.8 ± 0.0
Salix	39.6 ± 0.0	21.4 ± 0.4	27.1 ± 0.1	2.2 ± 0.0	29.2 ± 0.1	5.4 ± 0.0
Alnus	43.9 ± 0.5	26.7 ± 0.8	22.0 ± 1.1	2.9 ± 0.0	24.9 ± 0.0	3.4 ± 0.0
Alnus bark	16.3 ± 0.3	20.6 ± 0.0	43.6 ± 0.1	1.2 ± 0.0	44.8 ± 0.1	8.9 ± 0.3

2.3. Hydrochar via HTC

2.3.1. Experimental setup and procedure

HTC experiments were conducted in the 2 L high-pressure reactor (Parr series 4530 floor stand reactor). For each experiment, 65 g of driftwood was mixed with 1300 g of deionised water to obtain a solid to water (B/W) ratio of 0.5% following Yang et al. [54] and was then fed into the reactor. The B/W ratio was chosen to facilitate feeding and emptying the reactor and later hydrochar filtration. After that, the reactor was sealed and purged with N_2 for 2 min to remove the residual air. The reactor was then heated to the pre-set temperature (180, 200, 220 °C) for the desired residence time (4, 6, 12 h), which includes 30 min of heating at a rate of 2–3 °C.min^{-1}. At the end of the experiment, the reactor was left to cool down without intrusion. The pressure value in the reactor during the experiments was always higher than the saturation pressure. As a result, the water stayed in the liquid phase during the test.

The experiments were divided into two sections: impact of operational conditions, and impact of genera. Table 2 shows a summary of the operational conditions (temperature and residence time) for conducted experiments based on the genera and the associated pressure developed in the reactor. HTC was carried in duplicates and average. Hydrochar samples produced through HTC of driftwood were denoted as genius-temperature-residence time; for example, the *Alnus* sample prepared at 180 °C with a residence time of 4 h was labeled as *Alnus* 180–4. All the experiments were carried out in duplicates to obtain average values.

2.3.2. Mass and carbon balance

Gaseous products were released at the end of the experiment, and two samples of the produced gas were taken for analysis. Additionally, a liquid sample of approximately 75 g was collected for further analysis. The liquid-hydrochar mixture was then separated by filtration using three sieves (100, 45 and 20 μm) followed by washing the hydrochar with deionised water several times to remove impurities. The collected hydrochar was then dried in an oven at 105 °C for 24 h. All experiments were carried out in duplicates to obtain average values and ensure the reproducibility of the results.

The hydrochar mass yield was calculated based on the ratio between the mass of hydrochar obtained and the mass of biomass on a dry basis (db). Collected gas samples were analyzed in a gas chromatograph (GC) (SCION,456-GC) to identify the gas composition. The temperatures of the column oven, injector port, and were 30, 75, and 120 °C, respectively. The total gas mass produced was calculated following the ideal gas law and based on the pressure and the temperature when the samples were taken from the reactor and a vacant volume of 0.7 L. The gas yield was then calculated based on the ratio between the mass of gas obtained to the mass of biomass based on a dry basis. The estimation of the gas mass yield and carbon yield entailed an estimation of the vacant volume.

Total Organic Carbon (TOC) value of the produced liquid was measured. For each HTC run, the liquid obtained was ten times diluted in duplicates to obtain average values. TOC-V (Shimadzu) analyzer was used to measure the dissolved organic concentration in liquid samples using combustion methods at temperature 720 °C. The liquid yield was estimated based on the difference between the mass of biomass based on a dry basis and the hydrochar and gas yields. The carbon content in the liquid phase was calculated based on the TOC concentration, and a 1.3 L volume (water volume). This approximation could have impacted the final mass yield with around ± 0.4% based on an assumption of 500 kg·m^{-3} for hydrochar density. Carbon balance was developed based on the following equations.

$$C_{Total} = C_{Hydrochar} + C_{Gas} + C_{Liquid}$$

$$C_{Recovered} = \frac{C_{Total}}{C_{Biomass}}$$

2.3.3. Hydrochar characterization

Elemental composition (C, H, N, and S) was carried out following UNI 15104:2011 standard. Ash content was measured following UNI 14775:2010 standard. O was calculated based on difference. All measurements were done in quadruple for each hydrochar to obtain average values and to measure standard deviation.

Morphology of raw biomass and produced hydrochar were visualized with a scanning electron microscope (SEM). Each sample was coated with three layers of gold and platinum. Results obtained by SEM should be interpreted with caution since they were based on analyzing a small number of particles.

Table 2
Operational conditions used for HTC of the different driftwood genera.

Biomass	Temperature (°C)	Residence Time (h)	Pressure (bar)
Alnus	180	4, 6 and 12	11
	200	4, 6 and 12	16
	220	4, 6 and 12	25
Conifer	200	12	16
Fraxinus	200	12	16
Populus	200	12	16
Salix	200	12	16
Alnus bark	200	12	16

2.4. Hard carbon

2.4.1. Hard carbon production via pyrolysis

Between 5 and 9 g of hydrochar were placed in an alumina crucible and heat-treated for 1 h at 1400 °C, in a high-temperature oven. The selection of 1400 °C was based on previous research by Saavedra Rios et al. [36]. The treatment was done under an inert atmosphere (Ar, 15 L·h^{-1}) using a heating rate of 3·3 °C.min^{-1} (200 °C·h^{-1}). After treatment, the oven was set to cool down under argon until ambient temperature. Argon atmosphere was selected in order to assure an inert atmosphere at high temperatures and to avoid any possible N doping (as in the case of the N_2 atmosphere). The obtained powder was manually ground to obtain homogeneous particle size.

2.4.2. Hard carbon characterization

Scanning electron microscopy (SEM) images were obtained with a FEI Quanta 400 scanning electron microscope with a high-resolution low vacuum field emission gun (FEG).

The structure of the hard carbons was analyzed by several techniques: Raman Spectroscopy, X-Ray diffraction (XRD) and High-Resolution Transmission Electron Microscopy. Raman measurements were performed at room temperature using a LabRAM BX40 (Horiba Jobin-Yvon) spectrometer equipped with a He-Ne excitation source (532 nm wavelength). XRD analysis was performed using a D8 Advance Bruker AXS diffractometer with a copper cathode ($\lambda K\alpha = 15{,}418$ Å). The 2θ angle was varied from 5° to 80° using a step size of 0.05° and a counting time of 1 s. TOPAS software was used for the fitting of the patterns. HR-TEM images were obtained with a JEOL ARM-200 F instrument operating at 200 kV.

The textural properties of the hard carbons were studied with a Micromeritics ASAP 2420 instrument using both N_2 (77 K) and CO_2 (273 K) gases as adsorbates. Prior to analysis, the samples were outgassed for 12 h at 300 °C on the degassing ports and two additional hours on the analysis ports (300 °C). For each material, the Brunauer–Emmett–Teller (BET) specific surface area (SSA) was determined from the linear plot in the relative pressure (0.05–0.3) P/P_0 for N_2 and (0.01–0.03) for CO_2.

The chemical composition was assessed by Energy-dispersive X-ray spectroscopy (EDX) using a JED 2300 detector attached to an FEI Quanta 400 scanning electron microscope.

2.5. Na-ion batteries electrochemical performances

The electrochemical performances were investigated by galvanostatic cycling tests following the protocol described hereafter. Hard carbon was ground with a mortar below 100 μm before being used for electrode preparation. A slurry ink was made, composed of 90 wt% of hard-carbon active material, 5 wt% of carbon black C65 from IMERYS as a conductive additive and 5 wt% of PolyVinilydene DiFluoride (PVDF from Solvay) as the binder, in N-Methyl Pyrrolidone (NMP from Sigma Aldrich), It was then coated, using a doctor blade, onto an aluminum foil and dried at 55 °C overnight. Finally, it was cut into 14 mm diameter electrodes and dried under vacuum at 80 °C for 2 days.

Then, coin cells (CR2032) were assembled in an argon glove box using Na metal as a counter electrode. A CELGARD® 2400 membrane was used as a separator and a VILEDON® membrane was used to ensure electrolyte's accessibility. 150 μL of electrolyte was used. The latter is a solution of 1 M NaPF6 in ethylene carbonate (EC) with dimethyl carbonate (DMC) in a 1:1 vol ratio and addition of 1.5 wt% of fluoroethylene carbonate (FEC).

The cycling tests were performed using an Arbin Instruments battery cycler. The cells were cycled at a current density of 37.2 mA/g (C/10) during 5 cycles, and then at 372 mA/g (1 C) until the 100th cycle. We considered a theoretical capacity of C = 372 $mA{\cdot}g^{-1}$. Reduction (Na uptake in hard carbon)—oxidation (Na extraction from hard carbon) cycles ran between 3 V and 10 mV. At the end of each reduction, the cell was set to a constant voltage step of 10 mV. At least two-coin cells were tested for each hard carbon sample to check the repeatability of measurements.

3. Results and discussion

3.1. Conversion of river driftwood to hydrochar

3.1.1. Mass balance

Fig. 1 shows the mass yield (%) for hydrothermal carbonization. As expected, the predominant product of HTC was hydrochar in all experiments, whatever the studied operational conditions (temperatures and residence time) and wood genera.

These results are consistent with HTC experiments on wood at temperatures of up to 220 °C by Kang et al. [20]. For operational conditions experiments, hydrochar yield range was from 69% at 180–4 to48% at 220–12. In agreement with the literature, the hydrochar yield decreased with residence time and temperature under the conditions tested, and

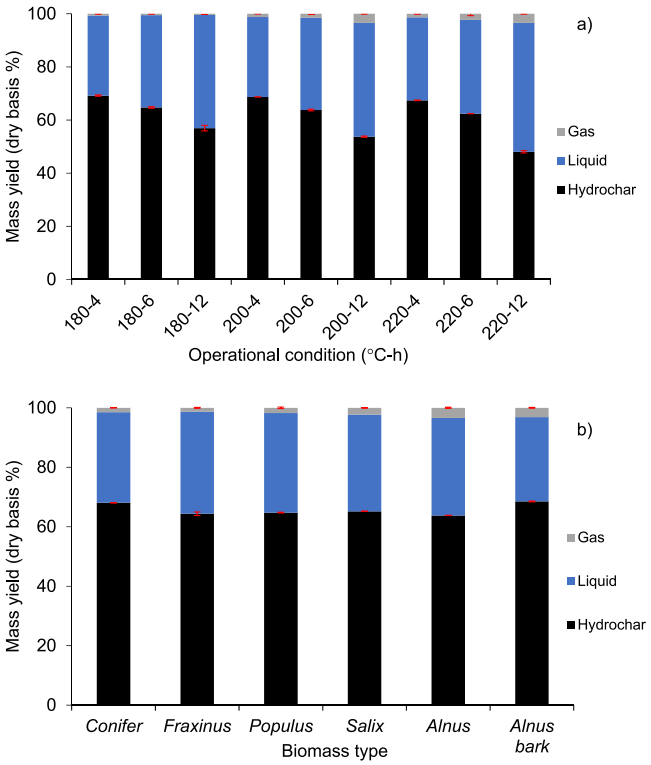

Fig. 1. Mass yields of HTC products of a. Alnus obtained at temperatures of 180, 200, 220 °C and residence times of 4, 6, 12 h, and b. driftwood biomass at a temperature of 200 °C and a residence time of 12 h.

the impact of temperature over the hydrochar yield was higher than the impact of residence time [29]. Indeed, at a relatively low temperature of 180 °C, HTC is known to degrade mostly hemicelluloses and limitedly degrade cellulose and lignin. The increase in temperature above 180 °C allows for more significant degradation of cellulose and an increase in the formation of secondary hydrochar, i.e., hydrochar produced by the degradation of liquid products from hydrolysis of wood.

Among genera, hydrochars yields vary significantly from 64% for *Fraxinus* to 69% for *Alnus* bark. This variation could be attributed to their macromolecular composition and ash leaching behavior. The high mass yield of *Conifer* compared to other deciduous wood can be explained by the composition of coniferous wood in general. Coniferous wood has been shown to have a higher lignin content compared to deciduous wood [32,42]. Klason lignin, in particular, is stable during HTC and requires high reaction severity with temperatures of approximately

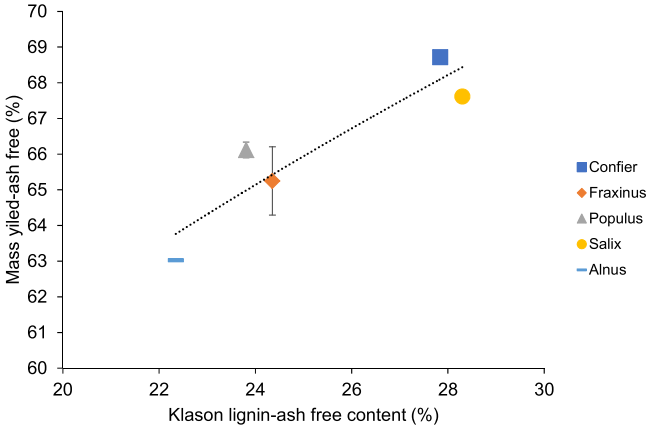

Fig. 2. Relationship between Klason-ligin and mass yield based on free ash content.

280 °C to degrade [20]. Fig. 2 shows the relationship between Klason-lignin ash free content with mass yield. Higher Klason lignin content led to a higher mass yield. The higher mass yield in coniferous supports Wilk et al. [51] study on the behavior of *Acaia* (deciduous) and Pine (coniferous) during HTC.

The gas product in both sets of experiments was significantly CO_2 (99%) as reported also by Basso et al. [2]. The absence of other gaseous compounds, such as CO and CH_4 eliminates the need for advanced gas treatment to comply with local regulations when large installations are considered. At different operational conditions, the CO_2 yield varied between 1% at 180 °C regardless of the residence time and 3% at 200–12 and 220–12. CO_2 production at a lower temperature of 180 °C was hardly impacted by the residence time. At a higher temperature of 200 and 220 °C, the increase in residence time led to an increase in the amount of gas produced while increasing temperature from 200 and 220 °C had a low impact on the gas produced.

Different driftwood genera led to significantly low CO_2 production and ranged from 1% for *Conifer* and *Fraxinus* to 3% for *Alnus* and *Alnus* bark. The relatively higher production of CO_2 could be attributed to a relatively higher partial elimination of mainly carboxyl groups to CO_2 in *Alnus* and *Alnus* bark [12,26].

The liquid mass yield was calculated, as explained in the materials and methods section, based on the difference. For operational conditions experiments, it accounts for 30% at 180–4 to49% at 220–12 of the total mass. As for the different driftwood biomass, the liquid mass yield was between 28% for *Alnus* bark and 34% for *Fraxinus*. The variation in liquid product yields among the studied operational conditions and genera can be attributed to their hydrochar mass yields. As the production of hydrochar increased, liquid production decreased. It is important to highlight that the produced liquid product is not a waste product and can be recycled leading to a higher hydrochar yield and C content [22,53]. Also, recycled liquid can be used for energy recovery by anaerobic digestion [28] or applied as a soil amendment [49].

3.1.2. CHONS composition and ash content

The CHONS composition and ash content of *Alnus* [32] and the hydrochar derived from HTC at different operational conditions are provided in Table 3. The physico-chemical characteristics of the various driftwood biomass [32] and the derived hydrochar obtained from HTC at a temperature of 200 °C and a residence time of 12 h are provided in Table 3. Standard deviations are provided when applicable. All measurements are based on a dry mass basis.

As expected, the increase of residence time and temperature led to an increase in C content compared to the raw biomass with values ranging from 49.9% for *Alnus* 180–6 to64.8% for *Alnus* 220–12. The obtained C content values correlate well with the C content of other hydrochars derived from woody biomass, which is usually in the range of 45–70% based on HTC reaction severity (temperature and residence time) [38,58].

H content decreased relatively from the original 6.5% present at the raw *Alnus* to a minimum of 5.5% at *Alnus* 220–12. Both the increase of temperature and residence time led to a decrease in H content. However, the impact of temperature was higher than residence time. N content in the produced hydrochar remained also relatively stable and low, ranging from 0.2 to 0.3%. The S content in all produced hydrochar was below 0.1%. Moreover, the O content decreased during HTC from 43.8% in the raw *Alnus* to 29.1% at 220–12. O content should be interpreted with caution because it is calculated based on the differences among the other elemental content; therefore, uncertainties of all measurements are added.

In the different studied genera, the C content in hydrochar obtained from the wood fraction of driftwood ranged 54.9% for *Alnus* to 57.4% for *Conifer*. The difference in C content could be attributed to the initial C content of the raw driftwood (48.8% for *Alnus* to 53.9/% for *Conifer)* and the driftwood macromolecules composition, most notably the lignin content.

H remained relatively stable among the different biomass with values from 5.8 to 5.9%. N content in the produced hydrochar remained relatively stable and low, with a maximum of 0.7% for *Alnus* bark. The S content in all produced hydrochar was below 0.1%. O content varied the most among the different studied biomass from 26.6% for *Alnus* bark to 40.4% for *Alnus*.

Table 3
CHONS composition and ash content on dry basis of Alnus and hydrochars derived following HTC.

Sample	Ash (%)	Elemental content (%-dry)				Atomic ratio	
		C	H	N	O	H/C	O/C
Alnus $_{raw}$	0.8	48.8±0.1	6.5±0.0	0.1±0.0	43.8	1.6	0.7
180-4	0.2	51.2±0.4	6.1±0.0	0.3±0.0	42.2	1.4	0.6
180-6	0.2	49.9±1.6	6.2±0.0	0.2±0.0	43.5	1.5	0.7
180-12	0.2	52.5±0.4	6.0±0.0	0.2±0.0	41.1	1.4	0.6
200-4	0.2	52.8±0.0	6.1±0.0	0.3±0.0	40.7	1.4	0.6
200-6	0.2	53.4±0.5	6.0±0.0	0.2±0.0	40.1	1.3	0.6
200-12	0.2	54.9±0.3	5.8±0.1	0.3±0.0	38.8	1.3	0.5
220-4	0.2	56.7±0.5	5.9±0.0	0.2±0.0	36.9	1.3	0.5
220-6	0.2	58.4±0.2	5.8±0.1	0.3±0.0	35.4	1.2	0.5
220-12	0.2	64.8±0.4	5.5±0.0	0.3±0.0	29.1	1.0	0.3

3.1.3. Ash content

Whatever the operational conditions tested, *Alnus* hydrochars had lower ash content than the raw material, going to a low value of 0.2%. On the other hand, HTC of the different driftwood biomass led to hydrochar with lower ash content than the raw biomass (0.2–1.4%) except for *Alnus* bark (8.0%). The relative decrease in ash content varied from 86% for *Fraxinus* to 36% for *Salix*. On the other hand, the ash content increased by 7% for *Alnus* bark.

HTC impact on hydrochar ash content seems to vary depending on the type of biomass and the ash composition. For woody lignocellulosic biomass, some inorganic elements leach into the liquid fraction. However, there is no agreement in the literature on the change in magnitude that occurs in the ash content [19,20].

Nevertheless, for the presented biomass, the reduction in ash content among the operational conditions and driftwood biomass might be attributed to different factors such as the increase in dielectric constant and the lower pH of the subcritical water [12,44]. However, the mechanisms behind inorganic element removal during HTC are complex, and to our knowledge not well-elucidated.

According to the ash composition analysis by Qatarneh et al. [32], Ca was the most abundant element (1607–6550 mg/kg) followed by K (69–1444 mg/kg). During HTC, Ca and K were probable to have leached while other elements, such as Fe, Mn, and Zn, remained in the hydrochar. The leaching behavior of K could be associated with their presence in the lignocellulosic biomass in the form of soluble ionic salts that ease their extraction during HTC with removal rates of 84–97% [33,44]. The removal of Ca is more complex and likely to be dependent on the type of lignocellulosic biomass and its original content that can reach a removal of up to 46% [33]. Si was partly leached and was inclined to remain in the hydrochar [33,44].

The results presented above regarding hydrochar produced from five main driftwood genera had similar ash content. Thus, hydrochar produced from HTC of river driftwood can be mixed for further application. The significant difference in the hydrochar obtained from the bark fraction can be neglected due to their low quantity and low presence in driftwood [32]. Moreover, obtained results are favorable for hard carbon application in Na-ion batteries since it was shown that high ash content could be problematic and strongly adverse influence electrochemical performances.

3.1.4. Carbon balance

Fig. 3 shows the C yield of HTC for operational conditions and driftwood biomass. The total recovered C among the different

operational conditions' accounts for 94–100%. On the other hand, the total recovered C among studied biomass accounts for 90–98% compared to C recovery of 94–98% by Oliveira et al. [28]. The total recovered C presents satisfactory elemental balance closure for such kinds of experiments. The C losses could be explained by possible spillage or droplet losses during filling and emptying the reactor and during the separation of hydrochar. Furthermore, the losses could also be due to the adhered hydrochar in the reactor walls and the assumptions made for the liquid and gas mass estimation.

The majority of the C from the raw biomass was concentrated in the produced hydrochar with 64–73% through HTC of *Alnus* at different operational conditions and 70–75% for various studied driftwood biomass. The C in the liquid product is the result of hydrolysis reactions, leading to the production of many organic compounds [45]. The liquid C yield between 24 and 29% for *Alnus* at different operational conditions and 16–24% for studied driftwood biomass. The low mass yield of gas produced during HTC accompanied a low C yield of less than 2% for all operational conditions and studied biomass.

3.1.5. Morphological properties

Obtained hydrochar particles from different operational conditions and driftwood biomass were highly heterogeneous in size, cross-section and morphology. The heterogeneity could be due to heat and mass transfer limitations during HTC. SEM micrographs presenting the impact of operational conditions and the different biomass are presented in the supporting information file.

As biomass begins to decompose, its fibrous structure is altered. The increase in temperature increased decomposition and reduced the amorphous structure. As a result, hydrochar with a smoother and less fibrous surface was produced. Even though these results differ from earlier studies by [50,52], they are consistent with those of Lucian et al. [24] and Gao et al. [13].

Graphs obtained from SEM show heterogeneity in microspheres formation. Microspheres are said to be rich in C and to be formed by nucleation growth mechanisms [40]. Their presence is hypothesized to be favorable for energy storage applications [27]. Therefore, microspheres are a positive characteristic of the hydrochars produced from driftwood in view of use in Na-ion batteries. Contrary to Simsir et al. [43], which could observe microspheres only when the residence time was longer than 12 h, in the present experiments, microspheres formation was observed even after 6 h of residence time. However, the aggregation of microspheres increased with residence time.

As for the different driftwood biomass, the formation of microspheres was observed in all studied biomass except for bark biomass. However, the reason behind the absence of microspheres in bark biomass is not clear. Microspheres number also varied among the different driftwood biomass from couple to tens of microspheres. For example, dense agglomeration can be seen in *Fraxinus* and *Salix* in the supporting information file.

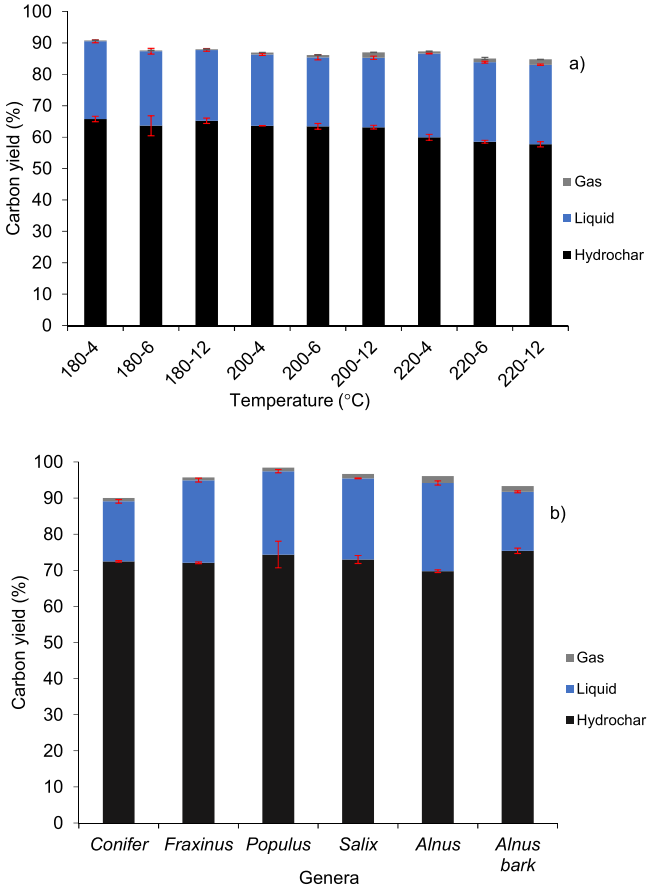

Fig. 3. C yield of HTC of a. Alnus b. Driftwood biomass.

3.2. Conversion of hydrochar into hard carbon

3.2.1. Hard carbon yield and morphology

Produced hydrochar was upgraded by a pyrolysis step at 1400 °C to produce hard carbon that is dense in carbon. Table 4 shows the hard carbon yield obtained for the different hydrochars after the thermal pyrolysis treatment. It is important to mention that the yield was determined based on the materials mass before and after pyrolysis and not from thermogravimetric analysis.

Starting with the hard carbons derived from the *Alnus* hydrochars obtained at different HTC operational conditions, the temperature used, and the residence time both have an influence on the final hard carbon yield which varies between 24 and 46%. Hard carbon yield tends to improve with the temperature increase from 180 °C to 220 °C (even if the residence time remains constant). Moreover, for the same temperature value (for example at 200 °C) the hard carbon yield improves when the residence time increases from 4 h to 12 h. As result, the hydrochar obtained at 220 °C and 12 h residence time led to the highest hard carbon yield (46%). The observed tendency can be linked to the initial hydrochar composition, which is richer in C% and poorer in O%

Table 4
CHONS composition and ash content on dry basis of the different driftwood biomass and the obtained hydrochar following HTC at a temperature of 200 ◦ C and a residence time of 12 h.

Sample	Ash (%)	Elemental content (%-dry)				Atomic ratio	
		C	H	N	O	H/C	O/C
Conifer $_{raw}$	0.7	53.9±0.0	6.1±0.0	<0.1	39.3	1.4	0.5
Conifer $_{hydrochar}$	0.2	57.4±0.2	5.9±0.1	0.2±0.0	36.3	1.2	0.5
Fraxinus $_{raw}$	1.1	49.5±0	6.3±0.0	<0.1	43.1	1.5	0.7
Fraxinus $_{hydrochar}$	0.2	55.4±0.2	5.9±0.0	0.2±0.0	38.3	1.3	0.5
Populus $_{raw}$	1.5	48.9±0	6.3±0.0	<0.1	43.3	1.6	0.7
Populus $_{hydrochar}$	0.5	55.0±0.7	5.8±0.1	0.2±0.0	38.5	1.3	0.5
Salix $_{raw}$	2.2	50.2±0.0	6.0±0.0	0.2±0.0	41.4	1.4	0.6
Salix $_{hydrochar}$	1.4	56.2±0.9	5.9±0.0	0.2±0.0	36.3	1.3	0.5
Alnus $_{raw}$	0.8	48.8±0.0	6.5±0.0	0.1±0.0	43.8	1.6	0.7
Alnus $_{hydrochar}$	0.2	54.9±0.3	5.8±0.1	0.3±0.0	38.8	1.3	0.5
Alnus bark $_{raw}$	7.4	53.5±0	5.9±0.0	0.8±0.0	32.4	1.3	0.5
Alnus bark $_{hydrochar}$	8.0	58.9±0.6	5.8±0.0	0.7±0.0	26.6	1.2	0.3

when the temperature and residence time increases (Table 3).

The driftwood biomass derived hard carbons produced a relatively similar yield (31–33%), except the *Alnus* bark which reaches a slightly higher value of 38%. As five materials are obtained at the same temperature (200 °C) and the same residence time (12 h), which explain the yields similarity. The slightly higher yield found for *Alnus* bark may be related to the hydrocarbon chemical composition which contains the highest C% (Table 4) among precursors. *Alnus* bark has the highest ash content, which contributes to the final higher yield.

In which concerns the morphology of the obtained hard carbons, four representative samples were evaluated by SEM, namely: *Conifer*, *Salix*, *Alnus* bark and *Alnus* 200.12. As a result of the high-temperature treatment, the materials lost almost entirely the initial fibrous morphology as can be seen in Supporting Information. Apart from the hard carbon derived from *Conifer*, which presents some large particles originating from the initial structure (Figure 9a, SI), one can see that the materials consist of very small particles of different sizes (2–100 μm) and shapes (mainly a random morphology). *Conifer* derived HC seems more heterogeneous than the other carbons with wider particle size distribution. The presence of microspheres that were initially observed in the case of several hydrocarbons (Figure 9b, SI) was also confirmed among the hard carbons, but very punctual.

3.2.2. Structural properties

Fig. 4a provides XRD characterization for the hard carbons produced under different operational conditions of HTC. XRD reveals a very similar hard carbon structure independent of the operational conditions of the HTC step. Hard carbon patterns present two characteristic peaks around $2\theta = 23°$ and $2\theta = 43°$. They correspond respectively to the graphene basal planes (002) and the perpendicular planes to the graphene layers (100). The position of the peak (002) is really similar for every material, between $2\theta = 22.8°$ and 23.0° which corresponds to an inter-layer distance d002 of 0.39 nm, which is higher than graphite (d_{002} = 0.335 nm) [25].

Similarly, XRD patterns in Fig. 4b reveal a very similar structure of five different woody fractions derived from hard carbons, with two characteristic peaks around $2\theta = 23.00°$ and 43.00°. The position of the (002) peaks lie between 22.71° and 23.84° 2θ for the woody fraction of *Conifer* and *Salix* respectively, which correspond to an interlayer space of 0.37–0.39 nm. It is sharper and shifted to the right at 25.69° for *Alnus* bark, which shows that the graphene layers are more organized and closer than the woody samples with d_{002} = 0.350 nm against 0.335 nm for the graphite.

Peaks on *Alnus* bark and *Salix* diffractograms highlight the presence of other Ca crystalline compounds: Calcite ($CaCO_3$ PDF 01–080–32–76) and Ca Carbide (CaC_2 PDF 04–015–4081) in *Salix* and Portlandite ($Ca(OH)_2$ PDF 00–044–1481) in *Alnus* bark. The two samples have higher ash and Ca content, as shown in Table 4 and Qatarneh et al. [32]. *Alnus* bark hard carbon contains more Ca compounds than *Salix,* as the height of the peaks reveals, which is in agreement with the very high amount of Ca in the raw material.

Similar to Saavedra Rios et al. [36] correlation between raw biomass inorganic composition and hard carbon structure, our results suggest that inorganic content in driftwood may have a strong influence on the structure of the resulting hard carbon. Si and Ca together catalyze the graphitization that could explain the right shifted *Alnus* bark hard carbon (002) peak XRD pattern.

Structural properties were evaluated, as well, by Raman spectroscopy and high-resolution transmission electron microscopy (HR-TEM). As above (SEM), the same four representative HC materials were considered since they present distinct structures as revealed by their d_{002} determined by XRD. Raman spectra (Fig. 5) confirmed the characteristic structure of hard carbon, as reported elsewhere [3]. Two sharp and intense peaks, corresponding to the defect-induced D-band and the crystalline graphite G-band, can be seen at approximately 1350 cm^{-1} and 1600 cm^{-1}, respectively. The ratio between the intensities of these two

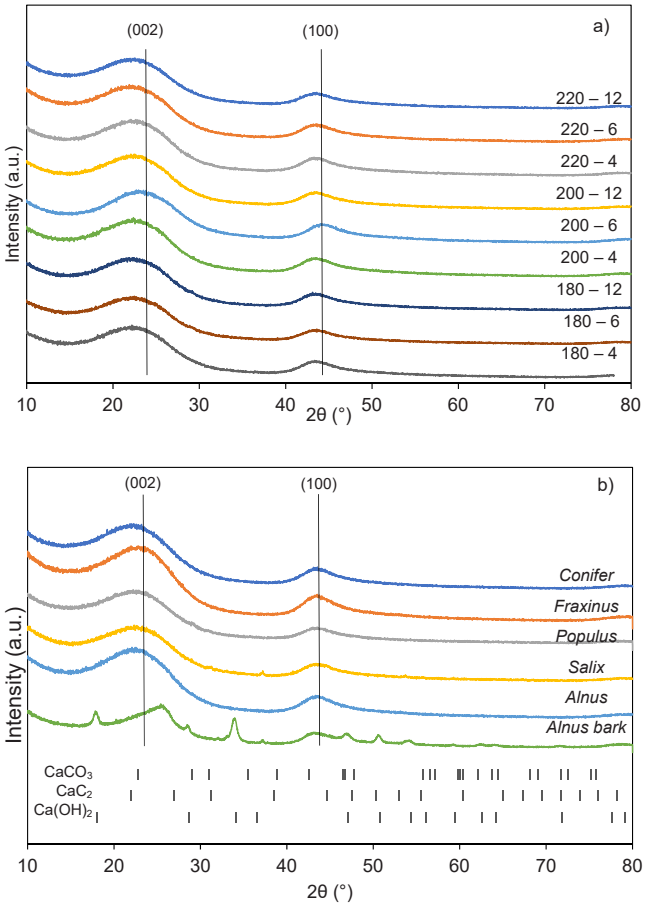

Fig. 4. XRD patterns for the different hard carbon from a. Alnus and b. driftwood biomass.

peaks can be used to quantify the disorder degree among the HCs (Fig. 5). The obtained values (1.23–1.58) imply a high disorder degree for all HCs, with a similar structure, as revealed by the normalized spectra which are alike. However, one can see that Alnus Bark derived HC has a slightly more organized structure, as suggested by both the I_D/I_G ratio which is lower, 1.23, and by the more intense 2D band in the 2500–3000 cm^{-1} region. This peak is characteristic of bulk graphite and

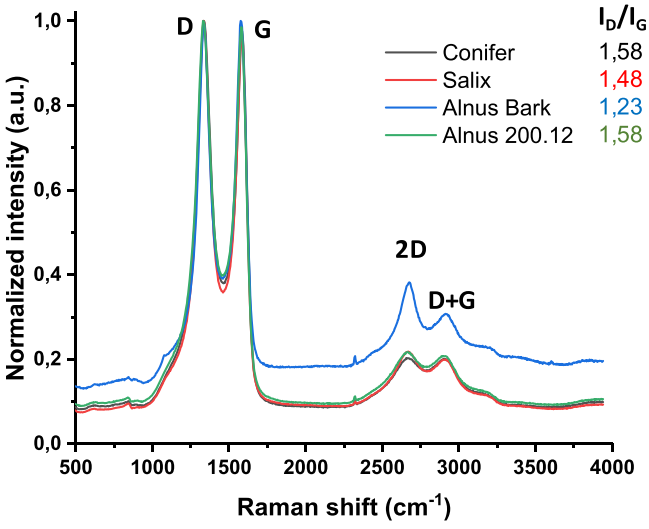

Fig. 5. Normalized Raman spectra of selected hard carbon materials and the corresponding I_D/I_G ratios.

therefore, linked to the degree of graphitization into the material. This result is in good agreement with the XRD showing the smallest d_{002} value for this carbon (d_{002} = 0.350 A).

Conversion of biochar into HC was also confirmed by HR-TEM images (Fig. 6) where randomly oriented curved graphene layers, similar to the "card house" model proposed by Dahn et al. [9] for hard carbons, could be seen. No significant structural difference could be seen among the materials. However, an important presence of impurities was noticed for Salix and Alnus Bark hard carbons (Fig. 6). To verify this aspect in more detail, Energy Dispersive X-Ray analysis was performed on the four materials and the results are presented in Table Y (Supporting Information). Traces of impurities were found for all HCs, including Ca, Cu, Si, S and Al, with higher weight percentages for Salix and Alnus Bark, which confirms HR-TEM observations. Calcium was found in higher content, especially for Alnus Bark HC (4.81 wt%), while for Salix 1.67 wt%. Because Ca is found in the form of an oxide, this leads to significant amounts of oxygen, (8.32 wt% and 12.11 wt%). Consequently, the amount of carbon is also lower for these two materials, 89.7 wt% for Salix and 82.9 wt% for Alnus bark. This might have an impact on the electrochemical performance since less carbon is available for Na insertion and the electronic conduction is lower [4] On the other hand, Conifer and Alnus 200.12 present only traces of impurities (< 0.3 wt%) and a lower quantity of oxygen. As result, the carbon amount is higher than 91 wt% for both materials.

3.2.3. *Textural properties*

Textural properties of the different hard carbons were revealed by gas adsorption-desorption measurements and the results are presented in Fig. 7. For most hard carbons, type II isotherms were obtained by N_2 adsorption-desorption analysis, specific for non-porous materials. This is also confirmed by the small volume of N_2 adsorbed. Differently, Alnus Bark shows slightly type IV isotherm, characterized by a hysteresis loop which may suggest the presence of a larger volume of mesopores in the structure, compared to other materials. This behavior can be related to the presence of high Ca-based impurities (4.18 wt%) which might induce catalytic activation with the formation of mesopores. Similar results have been observed in our previous work when using chitin as a precursor, and the possible activation reactions described therein [8]. BET specific surface area (SSA) was determined for all the hard carbons (Table 5) and the values were lower than 22 $m^2.g^{-1}$. This should be favorable to limit the undesirable reactions with the electrolyte. It is indeed established that hard carbons with high SSA result in high irreversible capacity during the first discharge-charge cycle [14].

No clear correlation could be established between HTC operational conditions and the resulting texture of hard carbons (Fig. 7a and c). However, materials treated under the least severe temperature of HTC (180 °C) seem to lead to hard carbons with a slightly higher SSA. As CO_2 gas has better accessibility for narrow pores due to its faster diffusion kinetics [14], the materials were analyzed by CO_2 adsorption, as well. Although the adsorbed volume is slightly higher than in the case of N_2, it remains low which denotes that the materials have very little porosity accessible. This is confirmed by the CO_2 SSA values found, which remain below 30 $m^2.g^{-1}$.

The adsorption measurements for the different driftwood biomass in

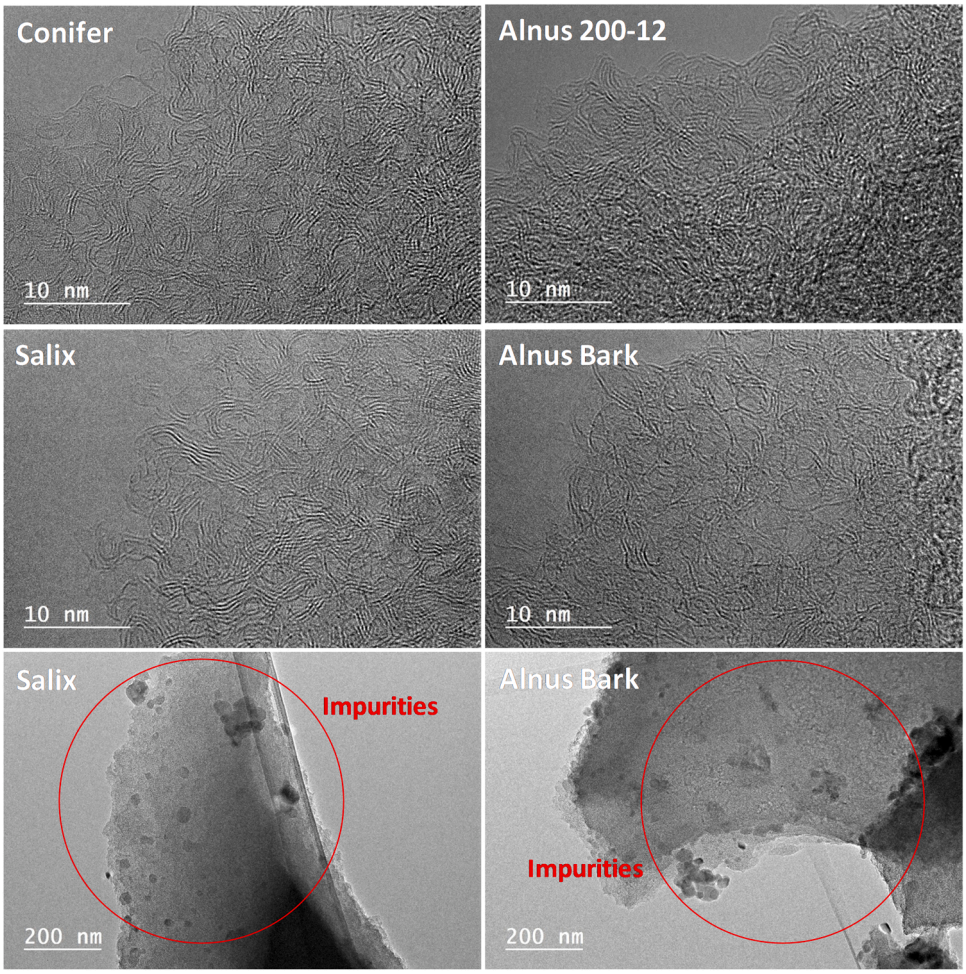

Fig. 6. HR-TEM images of selected hard carbon materials showing the turbostratic structure along with the presence of impurities in the case of Salix and Alnus Bark HCs.

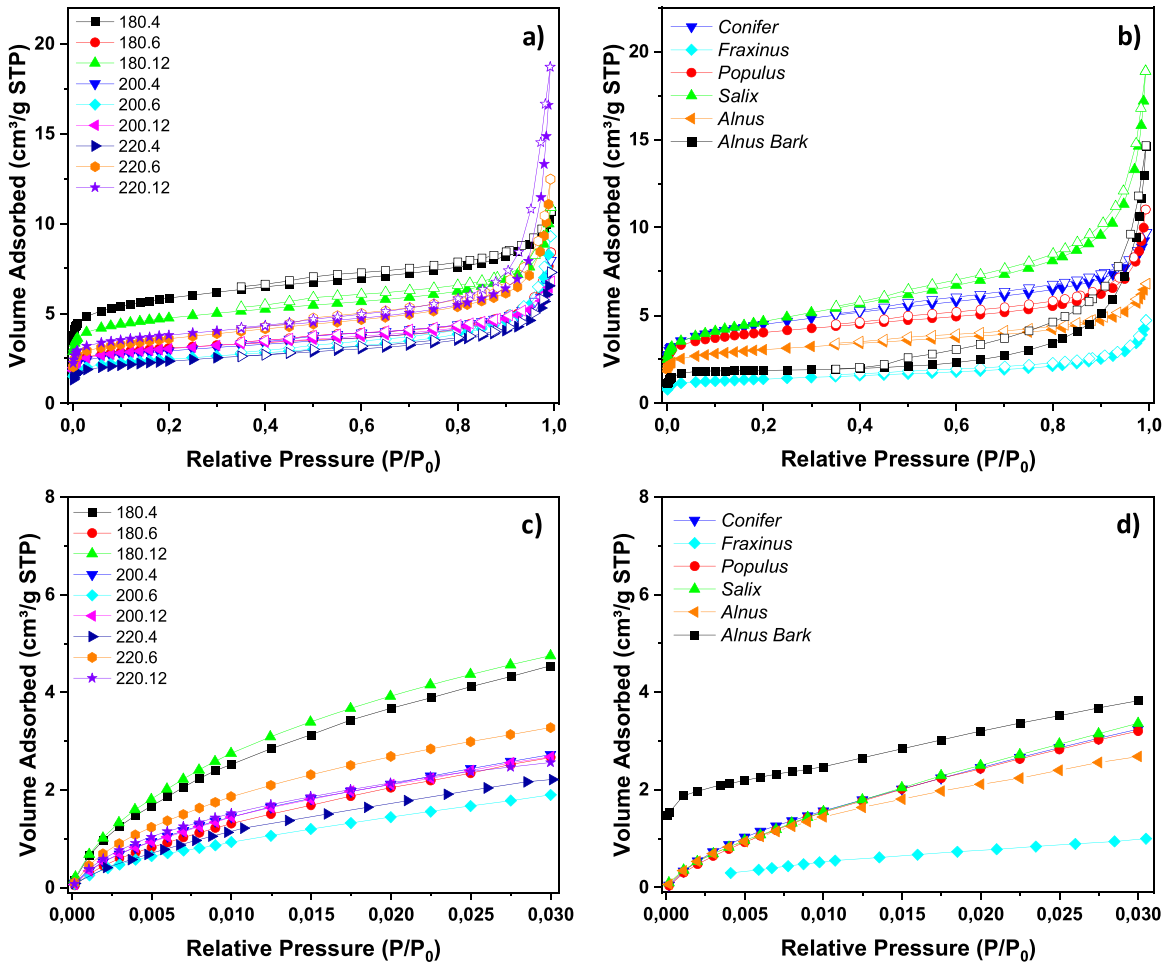

Fig. 7. N2 adsorption-desorption isotherms of hard carbon derived from a) Alnus and b) driftwood biomass, CO_2 adsorption isotherms of hard carbon derived from c) Alnus and d) driftwood biomass.

Table 5
Mass yield and specific surface area (SSA) obtained by N_2, and CO_2 adsorption analysis for hard carbon derived from river driftwood hydrochar.

Hard carbon	Yield (%)	N_2 SSA ($m^2.g^{-1}$)	CO_2 SSA ($m^2.g^{-1}$)	d_{002} (Å) Lc and La
180-4	24	21.5±0.0	26.5±1.0	3.88±0.05
180-6	24	11.3±0.0	17.7±0.9	3.87±0.05
180-12	26	17.5±0.0	27.7±0.6	3.88±0.05
200-4	26	10.7±0.0	16.5±0.7	3.84±0.05
200-6	29	9.0±0.0	11.5±0.7	3.77±0.05
200-12	31	11.1±0.0	16.1±0.7	3.86±0.05
220-4	32	8.4±0.0	15.6±0.7	3.86±0.05
220-6	38	13.0±0.0	19.2±0.6	3.89±0.05
220-12	46	14.0±0.0	14.6±0.4	3.87±0.05
Conifer	34	16.0±0.0	21.3±1.1	3.91±0.05
Fraxinus	32	5.0±0.0	6.9±0.2	3.81±0.05
Populus	31	16.4±0.0	23.4±1.7	3.87±0.05
Salix	33	14.7±0.0	23.1±1.1	3.83±0.05
Alnus	31	14.0±0.0	14.6±0.7	3.86±0.05
Alnus bark	38	7.5±0.0	17.8±0.8	3.46±0.05

Fig. 7b and d revealed non-porous materials, with very low specific surface areas. The type II adsorption-desorption N_2 isotherms revealed hard carbons with an SSA value between 5 $m^2.g^{-1}$ (*Fraxinus)* and 16 $m^2.g^{-1}$ (*Salix)*, which means low SSA for all driftwood biomasses. *Alnus* bark hard carbon has a very low SSA as well, and this might be related to the higher graphitization degree, i.e., more organized structure, as observed above with the XRD diffractogram. The same two materials have the smallest specific surface area when CO_2 adsorption gas was used. However, while for the *Alnus* bark hard carbon the value increased to 18 $m^2.g^{-1}$, the SSA of *Fraxinus* hard carbon remained almost stable (7 $m^2.g^{-1}$) denoting a compact material on which neither N_2 nor CO_2 can penetrate.

It seems difficult to clearly distinguish between the textural properties of the produced hard carbons. Although CO_2 gas has better diffusion kinetics, the results obtained are rather similar. A possible solution might be to approach a different gas probe, which can better access the complex porosity of hard carbon materials as recently reported in the literature [5]. In any case, in an application viewpoint, such results can be considered as positive, since it suggests that all types of driftwood could be suitable for conversion to Na-ion battery and there would be no need to separate the wood genera or remove the bark.

3.3. Electrochemical performances of hard carbons

The electrochemical performances of the cells consisting of hard carbons as an anode material are shown in Fig. 8. Whatever the HTC operational conditions and driftwood biomass, all hard carbons present similar behaviors both in the first cycle and upon cycling, in accordance with their similar physico-chemical and structural properties discussed above.

More precisely, the specific capacity during the first cycle was found to be between 270 and 300 $mAh{\cdot}g^{-1}$ and a related Coulombic efficiency

between 77% and 83%. These values are relatively higher than the obtained with other hard carbons derived from lignocellulosic hydrochars, such as 34% in peanut skin [47], 57% in shaddock peel [23], 72% in apricot shell [10], and 77% in reed straw [48]. Moreover, derived hard carbon can be compared with available commercial hard carbon such as PAC2 used in Na-ion battery prototypes with a specific capacity of 293 $mAh{\cdot}g^{-1}$ and a Coulombic efficiency of 86% ,which make driftwood potentially competitive [6]. In addition, the cyclability obtained was also promising, with a maximum of 2% of capacity loss after 100 cycles.

Only *Alnus* bark hard carbon appears as an outlier, with a much lower specific capacity of 167 $mAh{\cdot}g^{-1}$ and a Coulombic efficiency of 64%. This low performance can be related to a certain extent to the high content of impurities observed by EDX, especially to the high oxygen amount found in the materials, which favors solid electrolyte interface formation and leads to significant irreversible capacity in the first cycle. In addition, the lower quantity of C along with the narrow interlayer distance (0.350 nm) might limit the Na insertion and lead to lower capacity delivered. According to Cao et al. [7], a d_{002} of at least 3.7 Å is required for efficient Na insertion.

This result confirms the findings of Saavedra Rios [35] as well about the negative correlation between feedstock ash content and performance as an anode in Na-ion batteries. From a process viewpoint, such results would be in favor of removing bark from driftwood before conversion. However, such removal is partly made naturally during driftwood transport in rivers [30].

Based on 1300 tons the amount of wood available annually and the conversion yields presented above, the Génissiat dam can produce approximately 300 tons of hard carbon material. The produced hard carbon can be used in what is equivalent to 300 MWh of Na-ion batteries. When the published numbers of 3 million tons of driftwood extracted from 32 dams are considered [41], driftwood can produce approximately 1 million tons of hard carbon, meeting the annual 0.2-million-ton demand for battery-grade graphite [17].

4. Conclusion

The global efforts toward a greener economy are accompanied by an increase in demand for energy storage applications. Na-ion batteries with their cheaper and widely available resources, including hard carbon, are of great interest. We presented river driftwood as a potential resource for hard carbon. Unlike other waste, river driftwood has the advantage of lower ash content, few collection points with large quantities of wood, thus reducing the cost and energy-related to extraction and collection efforts. Obtained hard carbons showed promising electrochemical performance regardless of the previous HTC operational conditions and driftwood biomass used, except the bark fraction that is naturally removed during transportation of river driftwood. Tested anodes delivered a reversible discharge of 270–300 $mAh{\cdot}g^{-1}$ for the first cycle. Derived hard carbons had Coulombic efficiency of 77–83% and a promising cyclability of maximum 2% loss after 100 cycles. Results from this study suggest that utilizing global river driftwood can produce 1 million tons of hard carbon, meeting the annual 0.2 million ton demand on battery-grade graphite.

CRediT authorship contribution statement

Abdullah F. Qatarneh: Conceptualization, Methodology, Formal analysis, Investigation, Writing – original draft; **Capucine Dupont**: Conceptualization, Methodology, Writing – review & editing, Supervision, Funding acquisition; **Julie Michel** Formal analysis, Investigation; **Loïc Simonin** Methodology, Writing – review & editing; **Adrian Bedal** Formal analysis, Investigation; **Camelia Matei-Ghimbeu** Methodology, Writing – review & editing; **Virginia Ruiz-Villanueva** Methodology, Writing – review & editing; **Denilson da Silva** Writing – review & editing; **Hervé Piégay**: Conceptualization, Writing – review & editing, Supervision, Funding acquisition; **Mário J. Franca**: Conceptualization, Methodology, Writing – review & editing, Supervision.

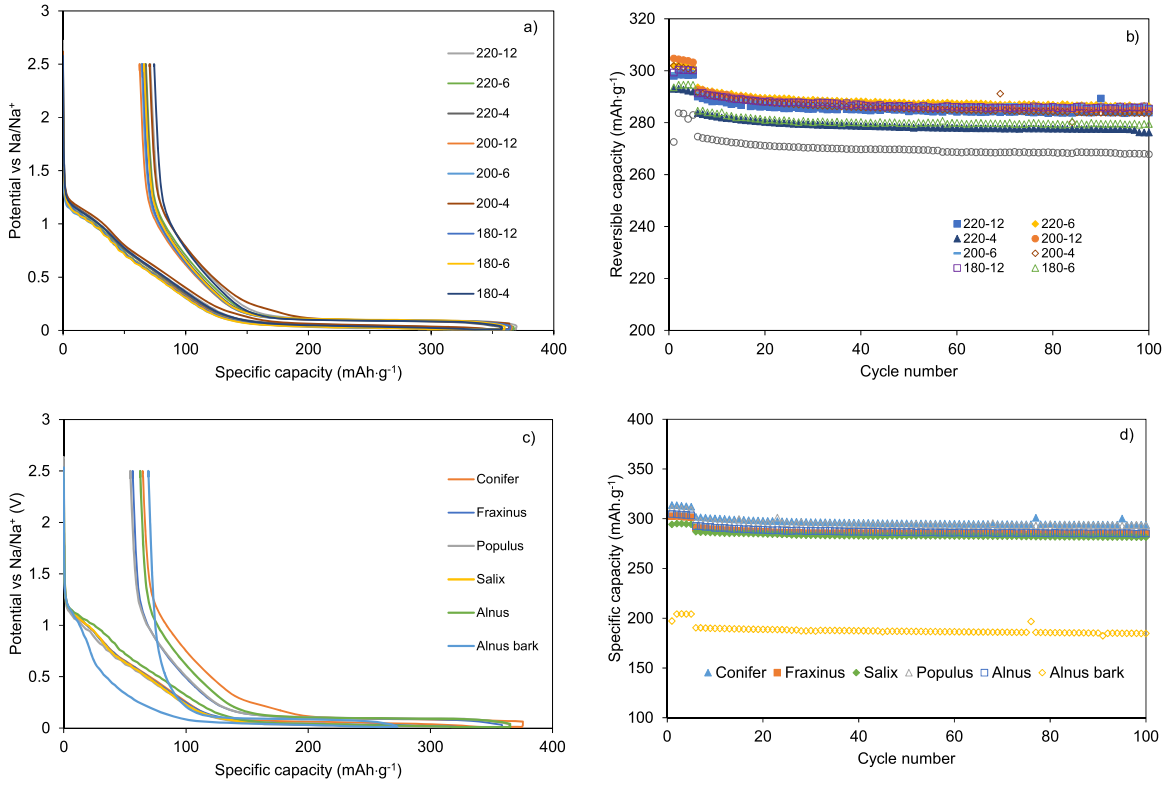

Fig. 8. Electrochemical results showing a. first cycle reduction-oxidation profile Alnus hard carbons b. stability of cycling for Alnus hard carbons C. first cycle reduction-oxidation profile driftwood biomass hard carbons d. stability of cycling for driftwood biomass hard carbon.

Declaration of Competing Interest

The authors declare that they have no known competing financial interests or personal relationships that could have appeared to influence the work reported in this paper.

Acknowledgement

We would like to thank ERAMUS MUNDUS for their support, Berend Lolkema for his assistance. In addition, we are grateful for the assistance and exchanges with IHE staff members, and CEA, France staff. This work was co-funded by the EUR H2O'Lyon (ANR-17-EURE-0018) of Université de Lyon, within the program "Investissements d'Avenir" operated by the French National Research Agency (ANR). This work was also co-funded by the European Union's Horizon 2020 research and innovation program NAIMA under grant agreement No 875629.

Appendix A. Supporting information

Supplementary data associated with this article can be found in the online version at doi:10.1016/j.jece.2021.106604.

References

[1] P. Bartocci, M. Barbanera, M. D'Amico, P. Laranci, G. Cavalaglio, M. Gelosia, D. Ingles, G. Bidini, C. Buratti, F. Cotana, et al., Thermal degradation of driftwood: determination of the concentration of sodium, calcium, magnesium, chlorine and sulfur containing compounds, Waste Manag. 60 (2017) 151–157.
[2] D. Basso, F. Patuzzi, D. Castello, M. Baratieri, E.C. Rada, E. Weiss-Hortala, L. Fiori, Agro-industrial waste to solid biofuel through hydrothermal carbonization, Waste Manag. 47 (2016) 114–121.
[3] A. Beda, P.L. Taberna, P. Simon, C.M. Ghimbeu, Hard carbons derived from green phenolic resins for Na-ion batteries, Carbon 139 (2018) 248–257.
[4] A. Beda, Le Meins, J.M. Taberna, P.L. Simon, P, Ghimbeu, C.M, Impact of biomass inorganic impurities on hard carbon properties and performance in Na-ion batteries, Sustain. Mater. Technol. 26 (2020), e00227.
[5] A. Beda, C. Vaulot, C.M. Ghimbeu, Hard carbon porosity revealed by the adsorption of multiple gas probe molecules (N_2, Ar, CO_2, O_2 and H_2), J. Mater. Chem. A 9 (2021) 937–943.
[6] A. Beda, F. Rabuel, M. Morcrette, S. Knopf, P.L. Taberna, P. Simon, C.M. Ghimbeu, Hard carbon key properties allow for the achievement of high Coulombic efficiency and high volumetric capacity in Na-ion batteries, J. Mater. Chem. A 9 (3) (2021) 1743–1758.
[7] Y. Cao, L. Xiao, M.L. Sushko, W. Wang, B. Schwenzer, J. Xiao, Z. Nie, L.V. Saraf, Z. Yang, J. Liu, Sodium ion insertion in hollow carbon nanowires for battery applications, Nano Lett. 12 (7) (2012) 3783–3787.
[8] J. Conder, C. Vaulot, C. Marino, C. Villevieille, C.M. Ghimbeu, Chitin and chitosan—structurally related precursors of dissimilar hard carbons for Na-ion battery, ACS Appl. Eng. 2 (7) (2019) 4841–4852.
[9] J.R. Dahn, W. Xing, Y. Gao, The "falling cards model" for the structure of microporous carbons, Carbon 35 (6) (1997) 825–830.
[10] E. Demir, M. Aydin, A.A. Arie, R. Demir-Cakan, Apricot shell derived hard carbons and their tin oxide composites as anode materials for sodium-ion batteries, J. Alloy. Compd. 788 (2019) 1093–1102.
[11] X. Dou, I. Hasa, D. Saurel, C. Vaalma, L. Wu, D. Buchholz, D. Bresser, S. Komaba, S. Passerini, Hard carbons for sodium-ion batteries: Structure, analysis, sustainability, and electrochemistry, Mater. Today 23 (2019) 87–104.
[12] A. Funke, F. Ziegler, Hydrothermal carbonization of biomass: a summary and discussion of chemical mechanisms for process engineering, Biofuels, Bioprod. Bioref. 4 (2010) 160–177.
[13] Y. Gao, X. Wang, J. Wang, X. Li, J. Cheng, H. Yang, H. Chen, Effect of residence time on chemical and structural properties of hydrochar obtained by hydrothermal carbonization of water hyacinth, Energy 58 (2013) 376–383.
[14] C.M. Ghimbeu, J. Gorka, V. Simone, L. Simonin, S. Martinet, C. Vix-Guterl, Insights on the Na^+ ion storage mechanism in hard carbon: discrimination between the porosity, surface functional groups and defects, Nano Eng. 44 (2018) 327–335.
[15] Gouton, C., 2018. Caracterisation du materiel ligneux provenant du bassin de l'arve afin de discriminer les sources et les evenements contributeurs. Master's thesis. Univeristy De Lyon. France.
[16] H. Hou, C. Yu, X. Liu, Y. Yao, Z. Dai, D. Li, The effect of carbonization temperature of waste cigarette butts on Na-storage capacity of N-doped hard carbon anode, Chem. Pap. 73 (5) (2019) 1237–1246.
[17] J. Huisman, T. Ciuta, F. Mathieux, S. Bobba, K. Georgitzikis, D. Pennington, Rmisraw materials in the battery value chain. Publications Office of the European Union, Luxembourg (2020).
[18] I. Izanzar, M. Dahbi, M. Kiso, S. Doubaji, S. Komaba, I. Saadoune, Hard carbons issued from date palm as efficient anode materials for sodium-ion batteries, Carbon 137 (2018) 165–173.
[19] J. Li, J. Zhao, P. Li, T. Lei, M. Yan, W. Ge, S, Pyrolysis behavior of hydrochar from hydrothermal carbonization of pinewood sawdust, J. Anal. Appl. Pyrolysis (2020), 104771.
[20] S. Kang, X. Li, J. Fan, J. Chang, Characterization of hydrochars produced by hydrothermal carbonization of lignin, cellulose, d-xylose, and wood meal, Ind. Eng. Chem. Res. 51 (2012) 9023–9031.
[21] Korpachev, V., 2004. Problems of prediction of pollution and clogging by woody mass and organic matter in reservoirs of high-pressure hydropower plants, in: Conference proceedings "Success of contemporary science"(in Russian).
[22] S. Leng, W. Li, C. Han, L. Chen, J. Chen, L. Fan, Q. Lu, J. Li, L. Leng, W. Zhou, Aqueous phase recirculation during hydrothermal carbonization of microalgae and soybean straw: a comparison study, Bioresour. Technol. 298 (2020), 122502.
[23] Ruizi Li, Jianfeng Huang, Zhanwei Xu, Hui Qi, Liyun Cao, Yijun Liu, Wenbin Li, Jiayin Li, Controlling the thickness of disordered turbostratic nanodomains in hard carbon with enhanced sodium storage performance, Eng.Tech. 6 (6) (2018) 1080–1087.
[24] M. Lucian, M. Volpe, L. Gao, G. Piro, J.L. Goldfarb, L. Fiori, Impact of hydrothermal carbonization conditions on the formation of hydrochars and secondary chars from the organic fraction of municipal solid waste, Fuel 233 (2018) 257–268.
[25] W. Lv, F. Wen, J. Xiang, J. Zhao, L. Li, L. Wang, Z. Liu, Y. Tian, Peanut shell derived hard carbon as ultralong cycling anodes for lithium and sodium batteries, Electrochim. Acta 176 (2015) 533–541.
[26] Ja Murray, D. Evans, The brown-coal/water system: part 3. thermal dewatering of brown coal, Fuel 51 (1972) 290–296.
[27] S.A. Nicolae, H. Au, P. Modugno, H. Luo, A.E. Szego, M. Qiao, L. Li, W. Yin, H. J. Heeres, N. Berge, et al., Recent advances in hydrothermal carbonisation: from tailored carbon materials and biochemicals to applications and bioenergy, Green. Chem. 22 (2020) 4747–4800.
[28] I. Oliveira, D. Blöhse, H.G. Ramke, Hydrothermal carbonization of agricultural residues, Bioresour. Technol. 142 (2013) 138–146.
[29] A.L. Pauline, K. Joseph, Hydrothermal carbonization of organic wastes to carbonaceous solid fuel–a review of mechanisms and process parameters, Fuel 279 (2020), 118472.
[30] H. Piégay, B. Moulin, C.R. Hupp, Assessment of transfer patterns and origins of in channel wood in large rivers using repeated field surveys and wood characterisation (the isère river upstream of pontcharra, france), Geomorphology 279 (2017) 27–43.
[31] Pillot, C., 2019. The rechargeable battery market and main trends 2018–2030, in: 36th Annual International Battery Seminar & Exhibit. Avicenne Energy.
[32] A.F. Qatarneh, C. Dupont, V. Ruiz-Villanueva, D. da Silva Perez, R.M. Ashour, H. Piégay, M.J. Franca, Evaluating river driftwood as a feedstock for biochar production, Waste Manag. 134 (2021) 197–205.
[33] M.T. Reza, J.G. Lynam, M.H. Uddin, C.J. Coronella, Hydrothermal carbonization: fate of inorganics, Biomass and Bioenerg. 49 (2013) 86–94.
[34] Cd.M.S. Rios, V. Simone, L. Simonin, S. Martinet, C. Dupont, Biochars from various biomass types as precursors for hard carbon anodes in sodium-ion batteries, Biomass and Bioenerg. 117 (2018) 32–37.
[35] Saavedra Rios, C.d.M. 2020a. Study of biomass-derived hard carbons for Sodium-ion battery application. Ph.D. thesis. Université Grenoble Alpes.
[36] Cd.M. Saavedra Rios, L. Simonin, Ad Geyer, C. Matei Ghimbeu, C. Dupont, Unraveling the properties of biomass-derived hard carbons upon thermal treatment for a practical application in Na-ion batteries, Energies 13 (2020) 3513.
[37] Sanders, M., 2017. Lithium-ion battery raw material supply and demand 2016–2025, in: Document presentado en the "Advanced Automotive Battery Conference", San Francisco.
[38] M.S. Santana, R.P. Alves, W.M. da Silva Borges, E. Francisquini, M.C. Guerreiro, Hydrochar production from defective coffee beans by hydrothermal carbonization, Bioresour. Technol. 300 (2020), 122653.
[39] F.H. Schweingruber, A. Börner, E.D. Schulze, Atlas of woody plant stems: evolution. structure, and environmental modifications, Springer Science & Business Media,, 2007.
[40] M. Sevilla, A.B. Fuertes, Chemical and structural properties of carbonaceous products obtained by hydrothermal carbonization of saccharides, Chem. Eur. J. 15 (2009) 4195–4203.
[41] O. Shumilova, K. Tockner, A. Gurnell, S. Langhans, M. Righetti, A. Lucía, C. Zarfl, Floating matter: a neglected component of the ecological integrity of rivers, Aquat. Sci. 81 (2019) 25.
[42] D. da Silva Perez, C. Dupont, A. Guillemain, S. Jacob, F. Labalette, S. Briand, S. Marsac, O. Guerrini, F. Broust, J.M. Commandre, Characterisation of the most representative agricultural and forestry biomasses in france for gasification, Waste Biomass-.-. Valoriz. 6 (2015) 515–526.
[43] H. Simsir, N. Eltugral, S. Karagoz, Hydrothermal carbonization for the preparation of hydrochars from glucose, cellulose, chitin, chitosan and wood chips via low-temperature and their characterization, Bioresour. Technol. 246 (2017) 82–87.
[44] A.M. Smith, S. Singh, A.B. Ross, Fate of inorganic material during hydrothermal carbonisation of biomass: Influence of feedstock on combustion behaviour of hydrochar, Fuel 169 (2016) 135–145.
[45] L. Suárez, I. Benavente-Ferraces, C. Plaza, S. de Pascual-Teresa, I. Suárez-Ruiz, T. A. Centeno, Hydrothermal carbonization as a sustainable strategy for integral valorisation of apple waste, Bioresour. Technol. (2020), 123395.
[46] R.F. Susanti, S. Alvin, J. Kim, Toward high-performance hard carbon as an anode for sodium-ion batteries: demineralization of biomass as a critical step, J. Ind. Eng. Chem. 91 (2020) 317–329.
[47] H. Wang, W. Yu, J. Shi, N. Mao, S. Chen, W. Liu, Biomass derived hierarchical porous carbons as high-performance anodes for sodium-ion batteries, Electrochim. Acta 188 (2016) 103–110.

[48] J. Wang, L. Yan, Q. Ren, L. Fan, F. Zhang, Z. Shi, Facile hydrothermal treatment route of reed straw-derived hard carbon for high performance sodium ion battery, Electrochim. Acta 291 (2018) 188–196.
[49] L. Wang, Y. Chang, Q. Liu, Fate and distribution of nutrients and heavy metals during hydrothermal carbonization of sewage sludge with implication to land application, J. Clean. Prod. 225 (2019) 972–983.
[50] T. Wang, Y. Zhai, Y. Zhu, C. Li, G. Zeng, A review of the hydrothermal carbonization of biomass waste for hydrochar formation: process conditions, fundamentals, and physicochemical properties, Renew. Sustain. Energy Rev. 90 (2018) 223–247.
[51] M. Wilk, A. Magdziarz, K. Jayaraman, M. Szymańska-Chargot, I. Gökalp, Hydrothermal carbonization characteristics of sewage sludge and lignocellulosic biomass. A comparative study, Biomass-.-. Bioenergy 120 (2019) 166–175.
[52] L.P. Xiao, Z.J. Shi, F. Xu, R.C. Sun, Hydrothermal carbonization of lignocellulosic biomass, Bioresour. Technol. 118 (2012) 619–623.
[53] Z.X. Xu, H. Song, P.J. Li, Z.X. He, Q. Wang, K. Wang, P.G. Duan, Hydrothermal carbonization of sewage sludge: effect of aqueous phase recycling, Chem. Eng. J. 387 (2020), 123410.
[54] G. Yang, S. Song, J. Li, Z. Tang, J. Ye, J. Yang, Preparation and CO_2 adsorption properties of porous carbon by hydrothermal carbonization of tree leaves, J. Mater. Sci. Technol. 35 (2019) 875–884.
[55] C. Yu, H. Hou, X. Liu, Y. Yao, Q. Liao, Z. Dai, D. Li, Old-loofah-derived hard carbon for long cyclicity anode in sodium ion battery, Int. J. Hydrog. Energy 43 (6) (2018) 3253–3260.
[56] H. Zhang, I. Hasa, S. Passerini, Beyond insertion for na-ion batteries: nanostructured alloying and conversion anode materials, Adv. Eng. Mater. 8 (2018) 1702582.
[57] T. Zhang, J. Mao, X. Liu, M. Xuan, K. Bi, X.L. Zhang, J. Hu, J. Fan, S. Chen, G. Shao, Pinecone biomass-derived hard carbon anodes for high-performance sodium-ion batteries, RSC Adv. 7 (66) (2017) 41504–41511.
[58] Z. Zhang, Y. Zhao, T. Wang, Spirulina hydrothermal carbonization: effect on hydrochar properties and sulfur transformation, Bioresour. Technol. 306 (2020), 123148.
[59] P. Zheng, T. Liu, X. Yuan, L. Zhang, Y. Liu, J. Huang, S. Guo, Enhanced performance by enlarged nano-pores of holly leaf-derived lamellar carbon for sodium-ion battery anode, Sci. Rep. 6 (1) (2016) 1–9.